

Numerical modelling of two-way reinforced concrete slabs in fire

Linus Lim^a, Andrew Buchanan^b, Peter Moss^b, Jean-Marc Franssen^c

^a*Holmes Fire and Safety, P. O. Box Q1643, QVB Post Office, Sydney, NSW, Australia*

^b*Department of Civil Engineering, University of Canterbury, Private Bag 4800, Christchurch, New Zealand*

^c*F.N.R.S., Dpt Mécanique des matériaux and Structures, Bât. B52/3 Chemin des Chevreuils, 1 4000 Liege 1 Belgium*

Abstract

This paper describes numerical modelling of the fire behaviour of two-way reinforced concrete slabs using a special purpose non-linear finite-element program, SAFIR. Several two-way reinforced concrete and composite steel-concrete slabs are tested under exposure to the ISO standard fire in order to validate the shell finite element in the SAFIR program. The modelling results showed agreement with the fire tests and demonstrate that the SAFIR shell element can be used to predict tensile membrane behaviour of two-way reinforced concrete slabs in fire conditions. The analyses show that two-way slabs have excellent fire resistance if they deform in double curvature and develop tensile membrane action.

Keywords: SAFIR; Finite-element analysis; Shell element; Fire resistance; Tensile membrane; Two-way slabs

1. INTRODUCTION

Recent fires occurring in steel framed buildings [1,2] have shown that unprotected composite steel-concrete floor slabs do not necessarily collapse during a compartment burnout despite being exposed to high temperatures and suffering considerable deformations. The slabs resisted collapse because they behaved as tensile membranes, supported by the colder perimeter beams and protected columns.

These fire tests have shown that steel framed buildings with concrete floor slabs have higher levels of fire resistance than would be expected from traditional considerations of fire resistance of steel and concrete structures [3]. This observation has led to computer modelling by numerous researchers [4-9] to better understand the behaviour of steel framed structures in fire and tensile membrane action in composite slabs.

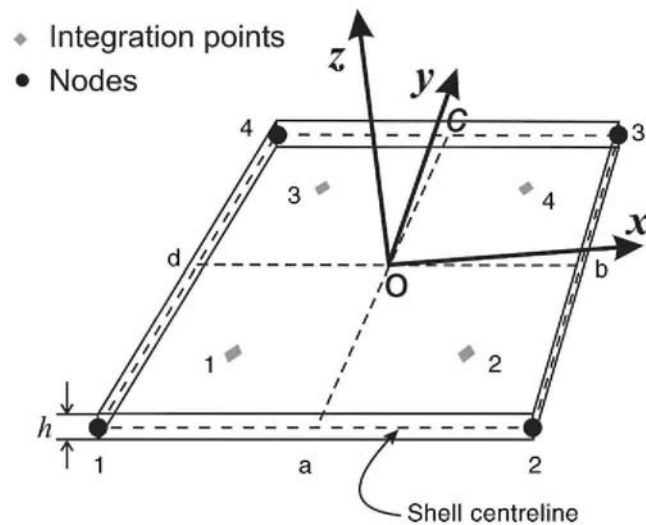
O'Callaghan et al. [9] have shown that the most accurate and efficient approach to modelling reinforced concrete slabs in fire is to perform 3D analysis incorporating shell finite elements. Shell elements can model slab behaviour because they account for the in-plane membrane forces in the slabs which play a very important role in supporting the loads. Several specialist and commercial finite-element programs such as VULCAN [10,11], ADAPTIC [12] and ABAQUS [13] have used shell elements to model reinforced concrete slabs in fire conditions.

The analyses carried out by previous researchers have concentrated mainly on the Cardington experiments. This was quite a complex structure that involved a lot of different structural phenomenon. This paper describes the computer analysis of simply supported two-way slabs in fire conditions using a special purpose finite-element program, SAFIR. The analysis was carried out to validate the performance of the concrete shell element in the SAFIR program by comparing the output with the results on several fire tests of two-way slabs. The fire tests were carried out by Lim and Wade [14]. The experimental tests and computer analyses were carried out to analyse a smaller, isolated structure, free from interactions with the surrounding structure. From a scientific perspective, this approach is more pure, allowing the research to be concentrated on the phenomenon in question. This paper presents some of the results of an extensive investigation on fire-exposed two-way concrete slabs [15]. One-way slab behaviour in fire was also included in the main study, but is beyond the scope of this paper.

2. THE SAFIR FINITE-ELEMENT PROGRAM

SAFIR [16] is a special purpose finite-element program developed at the University of Liege, Belgium, for analysing the behaviour of structures in fire. It is the successor to an earlier program, CEFICOSS, and consists of an integrated thermal and structural analysis program for performing non-linear 2D and 3D analyses of steel, concrete and composite structures in fire. SAFIR possesses a variety of finite elements such as beam, truss, solid and shell finite elements for modelling civil engineering problems. A four-noded shell element has recently been developed to model elements at ambient and fire conditions [17]. This new four-noded shell element supersedes an earlier triangular element shell element which performed well except when 'membrane bending' (i.e.: combined membrane and bending action) was involved in the analysis.

Fig. 1. Geometry of the shell element [16].



3. THE SAFIR QUADRILATERAL SHELL ELEMENT

3.1. Element formulation

The SAFIR shell element is a four node quadrilateral element. The shell element (Fig. 1) is defined by four corner nodes in the order of nodes 1-4, and has a constant thickness, h . The mid points of the edges of the elements are a , b , c and d while the centre of the local system of coordinates lies at the intersection, o , between a - c and b - d . The z -axis is perpendicular to the d - b and a - c plane.

There are four Gauss integration points on the surface of the shell element. There are also integration points distributed across the depth of the shell at the positions of the surface integration points. The number of Gauss integration points across the thickness is defined by the user, ranging from 2 to 10.

The shell element combines the membrane properties of a membrane element and flexural properties of a plate element. The properties of the plate element are based on the discrete Kirchhoff quadrilateral (DKQ) which is fully described elsewhere [18]. Some of the properties of the DKQ plate element are:

- The out-of-plane displacements and rotations are parabolic along each side.
- The contribution of the shear strain energy is neglected.
- To reproduce thin plate theory, the Kirchhoff condition is imposed at selected points. In this element, the Kirchhoff constraints are imposed along the edges. The shear strains at each of the two Gauss integration points along the sides are set to zero.
- The rotations along the edges vary linearly.

Some of the membrane properties of the shell element are:

- The element has a cubic membrane displacement field.
- The shear strains over the element are assumed to be constant.

3.2. Biaxial concrete model

A plane stress temperature dependent concrete model has been developed in SAFIR for modelling 3D reinforced concrete slabs using the shell element. The biaxial properties of concrete are modelled using a temperature dependent Von Mises plane stress associated plasticity model with a Rankine cut off in tension. The Von Mises surface is considered an adequate approximation for this purpose even though concrete in biaxial compression at elevated temperatures is known to have better behaviour than that predicted by the Von Mises surface [19]. A simple Rankine tension cut off has been used to model concrete in tension because even though there is some tension strength in concrete, for practical design applications, zero concrete tensile strength is usually recommended. Hence, a simple Rankine criterion is considered acceptable. The coefficients of thermal expansion of the concrete are based on those of the Eurocode 2 [20].

The evolution of Young's modulus and the isotropic hardening curve of the plane stress concrete model are chosen to match the uniaxial stress strain properties of concrete recommended by Eurocode 2 [20]. The hardening function, expressed by Eq. (1), allows elastic behaviour up to $\sigma_{eq} = 0.305f_c$ and has a finite slope at $\varepsilon_{pl,eq} = 0$. Details of the concrete model used in the shell element are presented elsewhere [21].

$$\left(\frac{3\varepsilon_{pl,eq}/\varepsilon_1 - 1}{1.0004} \right)^2 + \left(\frac{\sigma_{eq}}{f_c} \right)^6 = 1 \quad (1)$$

where $\varepsilon_{pl,eq,n}$ is the equivalent plastic strain, ε_1 the strain corresponding to peak stress, σ_{eq} the equivalent stress and f_c the concrete compressive strength.

3.3. Reinforcement

Reinforcing bars in the shell element are modelled based on a smeared model (i.e.: the unit area of the reinforcing steel is assumed to be a thin sheet of steel in each shell element.). The reinforcing layers in the shell elements can have any orientation in the local x - y plane. Each layer is defined by its local vertical coordinate in the shell and the orientation of the reinforcing relative to the local x -axis. Multiple layers of reinforcing bars can be defined in the shell element. Several assumptions for the reinforcing steel are:

- The cross-section of the rebar is not subtracted from the plane section of the element. This means that, in a reinforced concrete slab, steel and concrete are simultaneously present at the location of the bars.
- The bars resist actions parallel to the directions of the reinforcement. The reinforcing bars cannot directly resist shear forces.

3.4. Thermal analysis

The temperature distribution in the shell element is obtained from a SAFIR thermal analysis that has to be performed before the structural analysis. In most situations involving fire-exposed concrete slabs, the temperatures are assumed to vary only across the thickness of the element and are uniform across the plane of the slab. However, it is also possible to model a temperature field that varies across the plane and the thickness of the shell element.

3.5. Assumptions of the SAFIR analysis

Some of the assumptions of the SAFIR thermal and structural analyses are:

- Spalling of concrete cannot be modelled.
- SAFIR assumes full composite action between the concrete and the reinforcing steel and does not account for slip between the materials.
- SAFIR cannot model moisture migration in its thermal analysis but it accounts for the effects of moisture on the temperature distributions by using appropriate thermal properties.

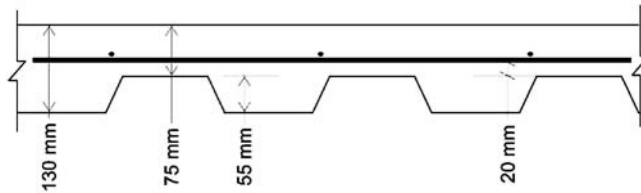
4. FIRE TESTS

The performance of the shell element with concrete properties in fire conditions has been validated by modelling two-way slabs in fire conditions. The results of fire tests of two-way slabs, carried out at BRANZ (Building Research Association of New Zealand) [14], are used for validation.

Table 1 Configuration of slabs

Slab	Thickness (mm)	Reinforcing steel area (mm^2/m)	Reinforcement fracture strain (%)	Concrete compressive strength, f'_c (MPa)
Flat slab	100	200	2.3	37
<i>Hi-bond</i> slab	130	200	2.3	32
<i>Speedfloor</i> slab	90	300	3.2	38

Fig. 2. Profile of the *Hi-bond* composite slab.



4.1. Slab properties

The three slabs that were tested comprised a reinforced concrete flat slab and two proprietary composite steel-concrete slabs. Each slab measured 3.3 m wide by 4.3 m long. The details of the slabs are shown in Table 1.

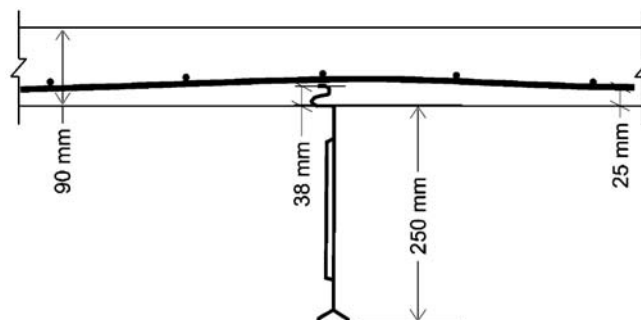
The *Hi-bond* slab is a proprietary composite slab with a trapezoidal profiled steel deck (Fig. 2), while the *Speedfloor* system is a reinforced concrete flat slab with suspended steel joists (Fig. 3), spaced at 1.3 m centres. The ribs of the *Hi-bond* steel decking and the joists of the *Speedfloor* slab spanned in the long direction of the slab.

Cold-drawn reinforcing mesh was used for the slab reinforcement. The fracture strains of the steel, determined from tensile tests at ambient conditions, are shown in Table 1. The yield stress of the mesh used in the flat slab and *Hi-bond* slab was 565 MPa. The yield stress of the mesh used in the *Speedfloor* slab was 568 MPa. The concrete compressive strengths shown in Table 1 are based on cylinder crushing tests carried out at ambient conditions.

4.2. Test configuration

The slabs were simply supported on rollers at all four edges over the furnace. The edges were horizontally unrestrained. The clear span between the supports in the long and short directions was 4.15 and 3.15 m, respectively. The corners of the slabs were clamped down to prevent curling and to more closely represent the behaviour of a slab under the support conditions of a real building. The slabs were each subjected to ISO fire exposure for 3 h while carrying a constant live load. The load was provided using twenty 200-l water drums to simulate a uniformly distributed live load of 3.0 kPa throughout the fire exposure.

Fig. 3. Profile of the *Speedfloor* composite slab.



4.3. Test results

All three slabs survived the 3 h ISO fire exposure without collapse. All the slabs deformed into double curvature, with the flat slab suffering the largest vertical deflection. All the slabs satisfied the insulation criteria for up to 1 h and 40 min. There was no spalling of the concrete during any of the fire tests.

Fig. 4 shows the measured midspan vertical deflections of the slabs during the fire tests. The slabs showed similar deflection trends during the fire, starting with a high deflection rate during the first 30 min, followed by a lower deflection rate at the later stages. The initial high deflection rate was caused by thermal bowing. The deflection rates decreased when the effects of thermal bowing decreased. The deflection rates of the flat slab and *Hi-bond* slab increased again during the final stages due to decreasing stiffness of the reinforcing steel. Fig. 4 shows that the *Speedfloor* slab had substantially smaller deflections at the end of the fire test, attributed to the joists which provided stiffness to the slab.

Fig. 5 shows the deformation of the *Hi-bond* slab after the fire test. The cold-drawn reinforcing steel in the heated slabs showed good behaviour and was able to resist the tensile forces in the middle of the slab without rupturing, indicating that the mesh gained significant ductility as the temperatures increased.

5. VALIDATION OF THE SHELL ELEMENT

The SAFIR shell element is used to model the three tested slabs. For both thermal and structural analyses, the concrete and reinforcing steel was modelled with material properties based on Eurocode 2 [20]. The low-ductility cold-drawn reinforcing mesh was modelled as 565 MPa hot-rolled reinforcing steel based on the assumption that the ductility of the cold-drawn mesh will increase when exposed to higher temperatures, hence behaving more like ductile hot-rolled steel. The concrete compressive strengths used for the analyses of the slabs were those shown in Table 1.

5.1. 100 mm flat slab

5.1.1. Thermal analysis

A thermal analysis was carried out using SAFIR to determine the thermal distribution in the concrete slab during the fire. A 2D thermal analysis was carried out, assuming that the temperatures in the slab varied only across the depth and were uniform at every height across the plane of the slab. The thermal analysis was performed by discretising a slice of the cross-section with solid elements (Fig. 6a) and subjecting the section to uniaxial heat flux from the bottom. A typical thermal distribution in the 100 mm slab is shown in Fig. 6b. It is assumed in the thermal analysis that the temperatures within the slab are not affected by concrete cracking which may be observed in the tests and predicted in the structural analysis.

Fig. 4. Midspan vertical deflections of the three slabs during the fire tests.

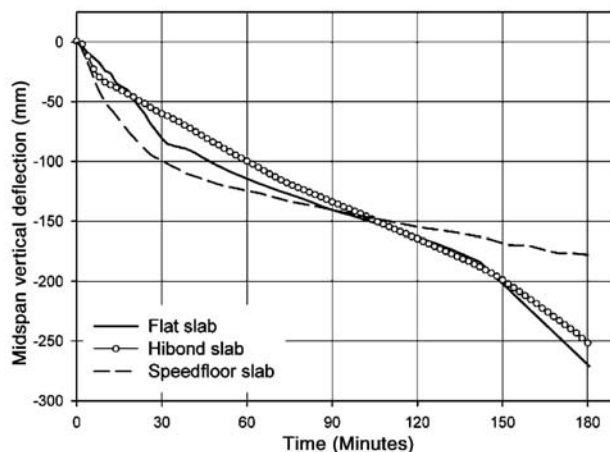
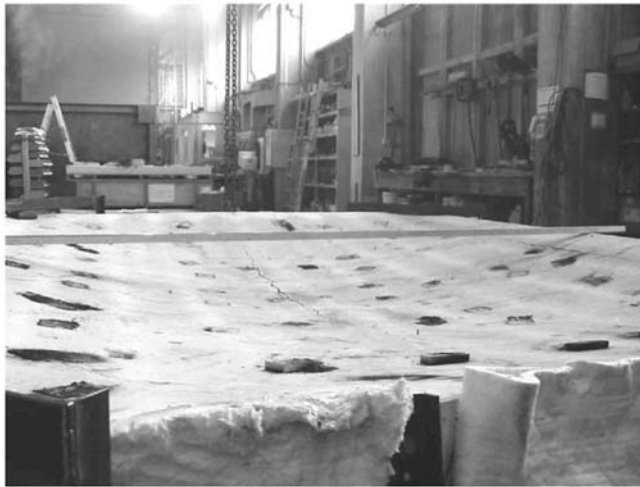


Fig. 5. Deformed shape of the Hi-bond composite slab after the fire test.



The variation of temperatures in the flat slab calculated with SAFIR and measured during the fire tests are shown in Fig. 7. The temperatures are plotted at the heated surface, middepth and the unheated surface of the slab. At the heated surface, the SAFIR predictions show good agreement with the experimental temperatures during the first 20 min but the measured temperatures drop off slightly and lag the SAFIR predictions for the remainder of the fire. At middepth (50 mm), the calculated temperatures show good agreement with the measured temperatures throughout the fire. At the top surface (100 mm), the SAFIR predictions initially show good agreement with the measured temperatures but predict slightly higher values later in the fire.

5.7.2. Structural analysis

The finite-element mesh used for the structural analysis of the 100 mm slab is shown in Fig. 8. A quarter of the full slab was modelled due to the symmetrical load and support conditions. The model, consisting of shell elements, includes both the heated region of the slab and the unheated edge of the slab (shown by the shaded region) which was located over the line of vertical support. A surface load of 5.4 kPa was applied to all of the shell elements, to model the vertical load consisting of the self-weight of the slab of 2.4 kPa, and the live load of 3.0 kPa. This applied surface load corresponds to a load ratio of approximately 0.40 for this flat slab.

Fig. 6. Thermal analysis of the 100 mm flat slab.

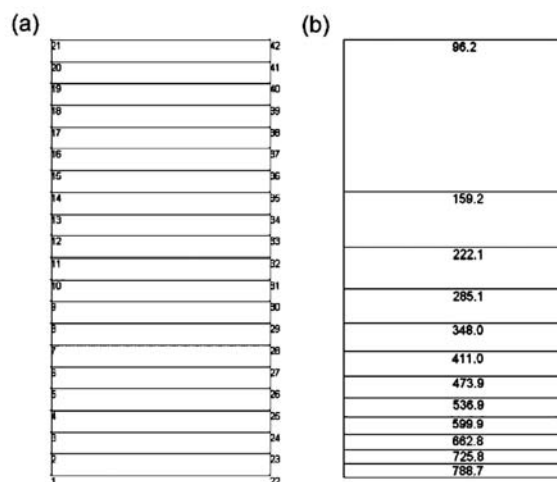


Fig. 7. Comparison of the measured and predicted temperatures in the flat slab.

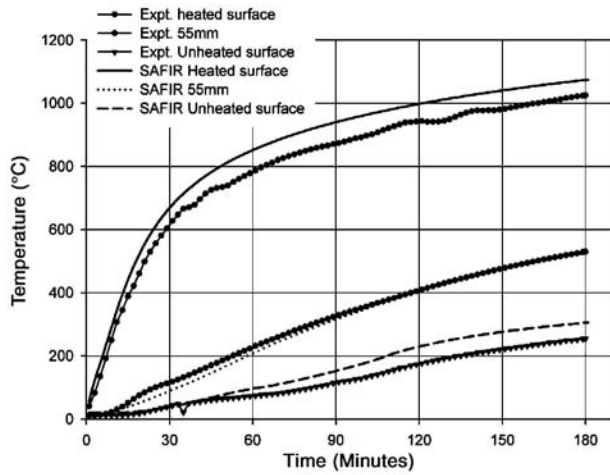
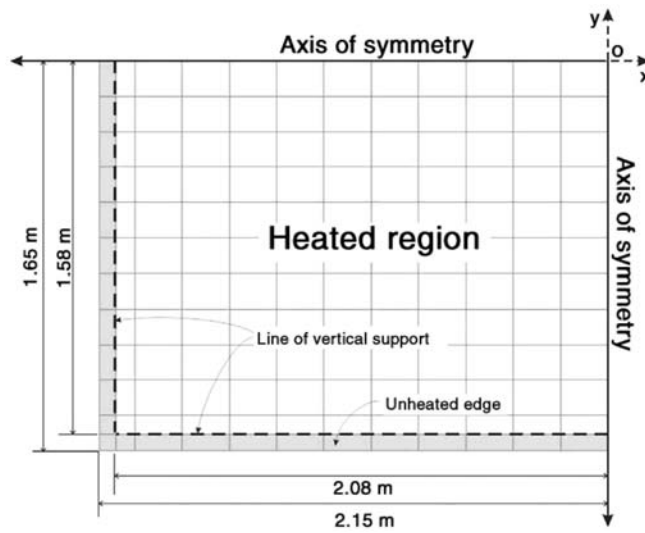


Fig. 8. Finite-element mesh for modelling the 100 mm flat slab.



5.1.3. Modelling results

Fig. 9 compares the SAFIR predictions of the flat slab with the experimental results. The slab was analysed with concrete tensile strengths of 0, 1.5 and 3 MPa. Zero concrete tensile strength corresponds to a slab that is fully cracked and 3.0 MPa corresponds to a slab with full concrete tensile strength, based on the equation $0.5\sqrt{f'_c}$, where f'_c is 37 MPa. An intermediate value of 1.5 MPa ($0.25\sqrt{f'_c}$) was also used.

The SAFIR analysis with zero concrete tensile strength predicts the deflection trend of the tested slab well, showing a high deflection rate during the first 30 min, followed by a gradual deflection rate up to 150 min, finally increasing again between 150 and 180 min. The predicted deflections are larger than the test results because the computer analysis assumed that the slab was fully cracked, such that the modelled slab possessed less stiffness than the actual tested slab.

With 1.5 MPa concrete tensile strength, the SAFIR results show good agreement with the test results for most of the fire duration. SAFIR predicts small deflections at the very start of the fire when the slab is uncracked, followed by thermal bowing deflection during the first 30 min of the fire. SAFIR predicts deflections very similar to the test results up to 150 min but underestimates the test results during the final 30 min. The deflected shape of the slab predicted with SAFIR after 3 h fire exposure is shown in Fig. 10.

The deflections predicted by SAFIR using 3 MPa concrete tensile strength show good agreement with the experimental test results during the first 100 min. Beyond that, the deflections diverge as the predicted

deflections asymptote to -200 mm, while the experimental deflections continue to increase. The lower deflections predicted by SAFIR using 3 MPa concrete tensile strength is possibly due to the concrete model not modelling sufficient cracking at this level of high concrete tensile strength.

The analysis of the two-way slabs shows that the deflections are sensitive to the concrete tensile strength. Large values of concrete tensile strength lead to under-prediction of the deflections of the tested slab, particularly during the advanced stages of the fire. If zero concrete tensile strength is used, the predicted deflections are larger than the test results; nevertheless, the deflection trend is consistent with the test results and can be used as a conservative estimate of the slab behaviour.

5.1.4. Distribution of membrane tractions in the flat slab

The distribution and orientation of the principal membrane forces in the slab during the fire, calculated using SAFIR, are shown in Figs. 11-13. The membrane tractions are plotted for the slab analysed with 1.5 MPa concrete tensile strength. Compressive membrane tractions are shown as thick dark arrows, while tensile membrane tractions are represented by light thin arrows. The lengths of the arrows indicate the magnitude of the membrane tractions.

Fig. 11 shows that at ambient conditions, the calculated membrane tractions in the slab are very low.

Fig. 9. Midspan vertical deflections with different values of concrete tensile strength.

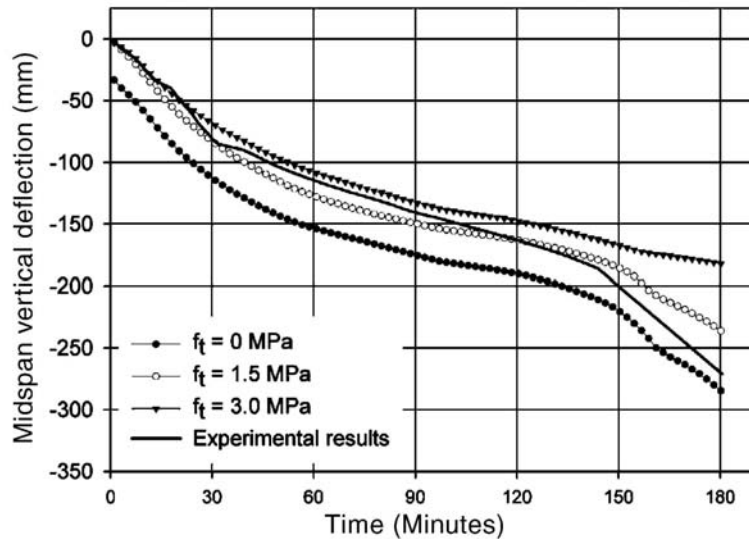


Fig. 10. Deflected shape of the slab at 3 h (magnified 1.5 times).

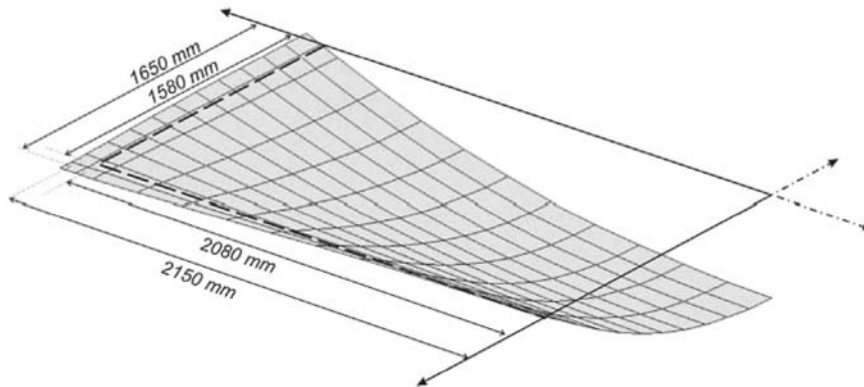


Fig. 11. Membrane force distribution at ambient conditions.

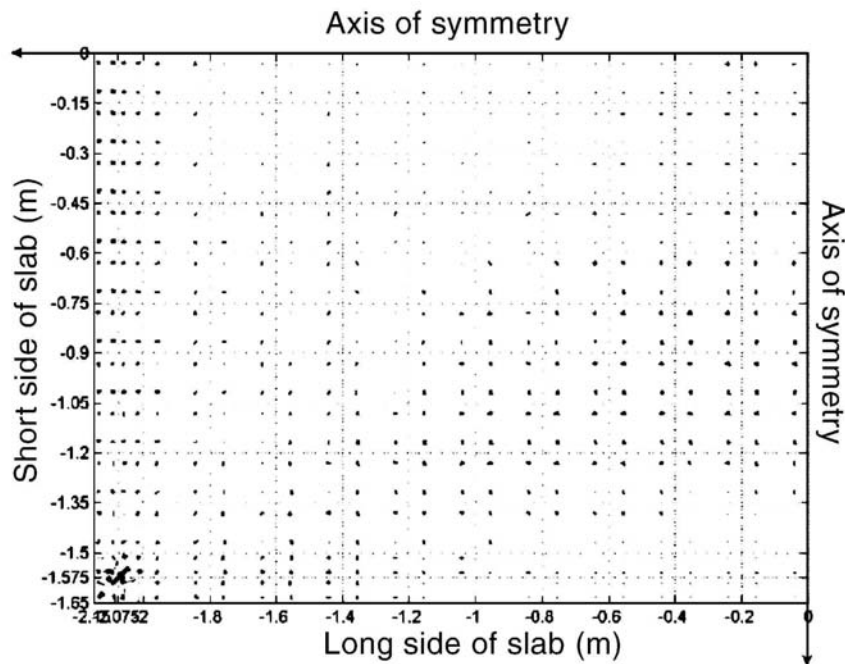
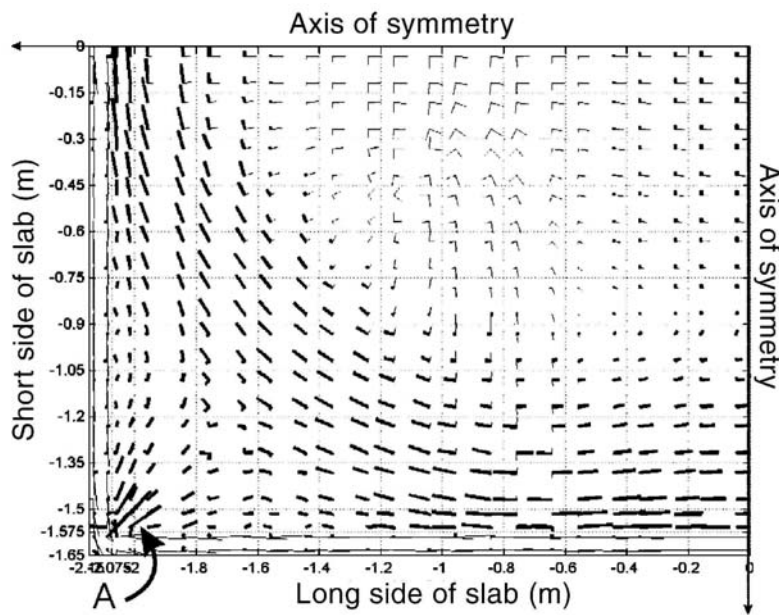


Fig. 12. Membrane force distribution after 30 min fire exposure.



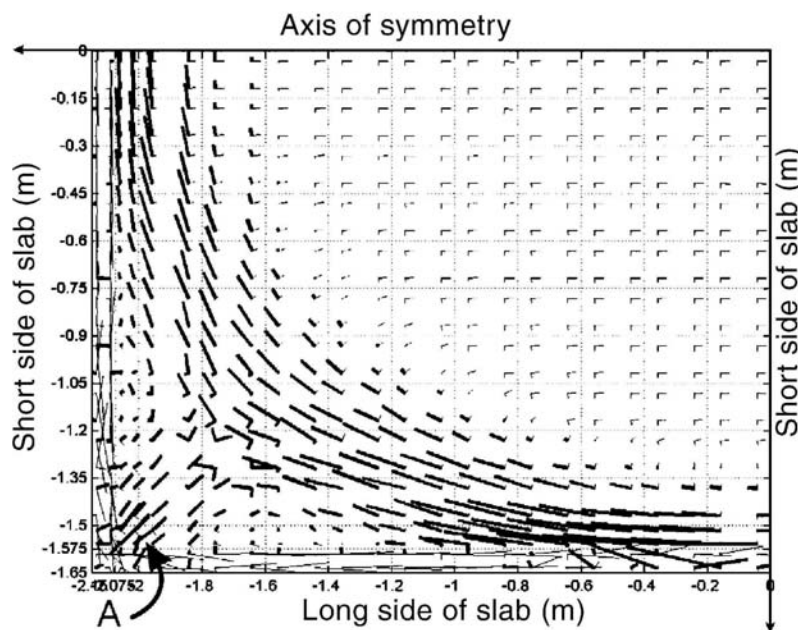
At this stage, the loads on the slab are resisted by bending action. Fig. 12 shows that after 30 min of fire exposure, the analyses predict significant membrane forces in the slab. The corresponding midspan deflection predicted by SAFIR at this stage is 83 mm. The membrane tractions in the slab consist of a tension field in the centre surrounded by a compression ring at the edges of the heated region. This distribution of the membrane tractions is attributed to the deflected shape of the slab; the sagging midspan deflections produce tension tractions in the midspan region which are resisted by the compression membrane tractions at the outer perimeter of the heated section.

The heated region of the slab is confined by a thin tension ring at the unheated outer edges which resists the thermal expansion of the heated central region. In the test, the tensile membrane tractions in the outer unheated edges were resisted by perimeter trimmer bars built into the slab. Fig. 12 shows that large compressive forces form at the corner support (marked A) due to the tensile ring restraining the expansion of the heated central region.

After 3 h, Fig. 13 shows that the width of the compression ring decreases noticeably and shifts to the unheated outer edges along the centre of the long span (Point B). The magnitude of the compression membrane tractions at this region had increased very significantly. However, the magnitude of the tension tractions in the central midspan region of the slab has decreased markedly due to the decreasing strength of the reinforcing mesh. The analysis shows that the development of tensile membrane action results in good behaviour and high fire resistance of the slab.

The SAFIR analysis showed that the slab develops tensile membrane behaviour from the early stages of the fire as a result of the large vertical deflections which were caused by thermal bowing, unlike a slab at ambient temperatures with increasing load, which only develops tensile membrane action when it approaches failure and after yield lines have formed. Observations of the slab during the fire test [14] showed that the slab suffered superficial cracking during most of the fire duration and that yield line cracks appeared during the advanced stages of fire exposure.

Fig. 13. Membrane force distribution after 3 h fire exposure.



5.2. The Speedfloor composite slab

The *Speedfloor* slab, which comprised a reinforced concrete flat slab and steel joists, was modelled using shell and beam finite elements. The flat slab was modelled in a similar manner to the flat slab, while beam finite elements were used to model the steel joists. The properties of the 3D SAFIR beam element are presented elsewhere [16,22]. The properties of the concrete and reinforcing in the *Speedfloor* slab are based on the tested slab. Similar to the flat slab, the reinforcing mesh was modelled using hot-rolled reinforcing properties based on Eurocode 2 [20]. The loading and support conditions of the *Speedfloor* slab are identical to those used to model the flat slab.

5.2.1. Thermal analysis

For the thermal analysis, the concrete slab and a single steel joist embedded in a slice of the 90 mm thick concrete slab were modelled, as shown in Fig. 14a. The steel joist was exposed to three-sided heating, while the

slab was only heated at the bottom surface. Fig. 14b shows the temperature distributions in the slab after an hour of exposure to the ISO fire. It shows very high temperatures in the exposed joist, while the embedded steel in the slab was relatively cool.

5.2.2. Structural model

Fig. 15 shows a schematic of the cross-section of the *Speedfloor* slab for the structural analysis. It comprises beam elements, which represent the joists, and shell elements which form the slab. To model composite action between the beam and shell elements, the nodeline of the beam element was aligned with that of the shell element. The joist of the beam element was modelled with hot-rolled steel properties based on Eurocode 3 [23]. The beam element consists of the steel joist and the concrete slab. However, the concrete in the beam element was modelled with non-load-bearing properties (zero strength and modulus of elasticity) so that it did not contribute to the strength and stiffness of the slab, which was already provided by the shell elements.

Fig. 16 shows a plan view of the finite-element mesh for the structural analysis of the *Speedfloor* slab, which consists of shell and beam elements. Half of the *Speedfloor* slab was modelled due to the asymmetric cross-section of the joist located at the centre of the slab.

Fig. 17 compares the midspan vertical deflections predicted by SAFIR with the experimental results. The analysis of the *Speedfloor* slab was performed with 0 and $0.25\sqrt{f'_c}$ concrete tensile strength. $0.25\sqrt{f'_c}$ concrete tensile strength was used because it showed fairly good representation of the actual tensile strength of the concrete, as shown in analysis of the flat slab. The graph shows that SAFIR predicts the deflection trend of the tested slab fairly well throughout the fire duration. The analysis with zero concrete tensile strength underestimates the deflections between 12 and 66 min but slightly over-predicts the deflections after 120 min. With 1.55 MPa concrete tensile strength, the analyses slightly underestimate the test deflections for the entire fire duration but show agreement in predicting the deflection trend. Even though the steel joists have lost significant strength and stiffness due to the high temperatures, they do reduce the deflections of the *Speedfloor* slab, and the SAFIR analysis predicts this reasonably accurately.

Fig. 14. Finite-element mesh and typical thermal gradients in the *Speedfloor* slab.

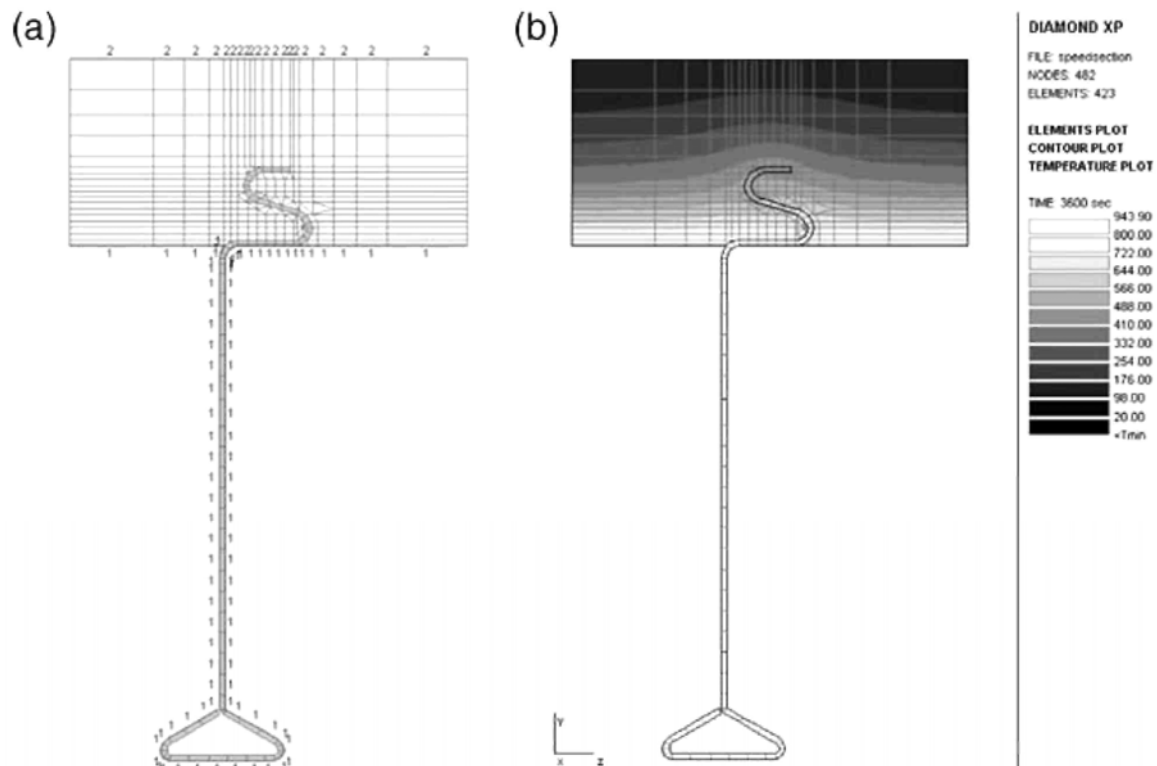


Fig. 15. Discretisation of the Speedfloor cross-section for structural analysis.

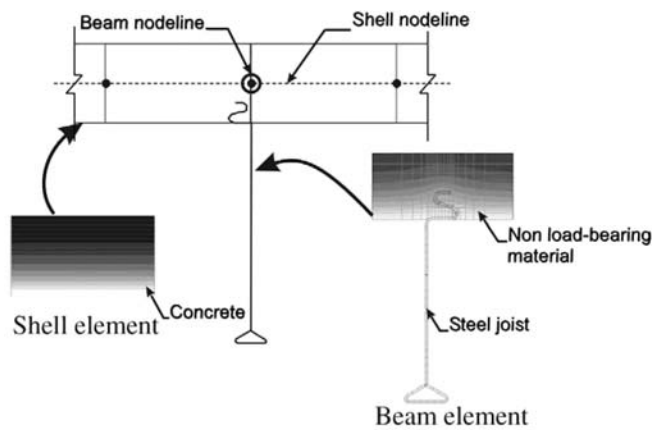


Fig. 16. Finite-element discretisation of the Speedfloor slab with beam and shell elements.

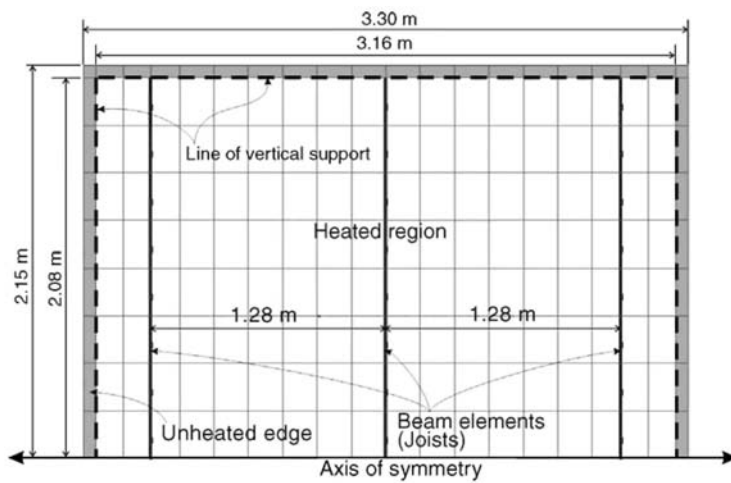
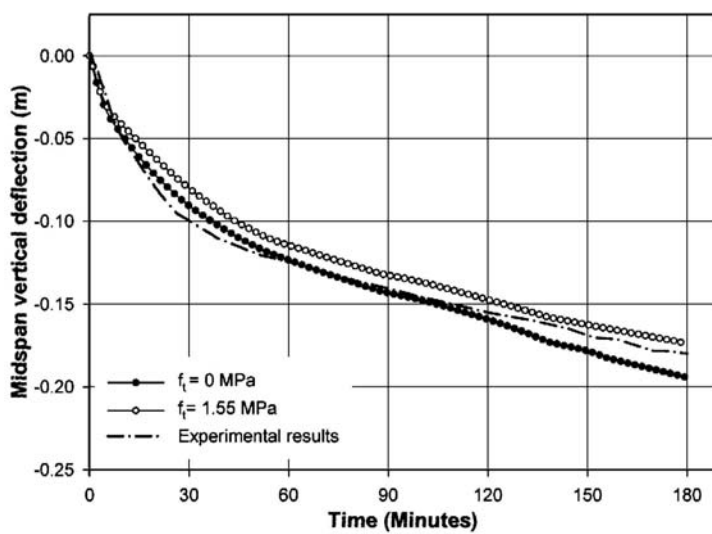


Fig. 17. Midspan vertical deflections of the Speedfloor slab during the ISO fire.



5.3. Hi-bond composite slab

5.3.1. Thermal analysis

For the *Hi-bond* slab, the thermal analysis had to consider the different temperatures across the thick and thin sections of the slab. Fig. 18a shows the temperature gradients from a conventional thermal analysis of the section. To allow for the subsequent structural analysis, a combination of shell elements and beam elements with different temperature exposures had to be used, as shown in Fig. 18b. Two shell elements, labelled *Shell A* and *Shell B*, were used to model the temperatures in the thin and thick sections, respectively. The underside of *Shell A* is directly exposed to the ISO fire, while the underside of *Shell B* is exposed to a uniform lower temperature-time curve obtained from position X of Fig. 18a which provided a good estimate of the temperature variation above the trough. Temperature gradients in the trough were obtained from thermal analysis of the beam element, with ISO fire heating on the exposed surfaces.

Fig. 19 compares the temperatures in the *Hi-bond* slab calculated using SAFIR with the temperatures obtained from the fire tests. The temperatures from the tests and SAFIR were measured in the centre of the trough, as shown in Fig. 18b, at various distances from the bottom of the steel decking. At the bottom of the trough (0 mm), SAFIR predicted a similar trend to the ISO fire, starting with a high linear rate of temperature rise followed by a lower, non-linear rate of temperature rise. The temperatures of the tested slab were lower during the first 18 min but showed a similar trend for the remainder of the fire, lagging the calculated values throughout the fire. Numerical modelling of similar slabs by other researchers [24] has also shown that measured temperatures at the bottom surface during a fire are substantially lower than those predicted by computer analysis. This difference is probably caused by the steel decking on the bottom surface buckling and debonding from the concrete slab. The debonding of the steel deck, possibly due to steam release at the bottom of the slab, creates an insulating layer of air between the decking and the concrete. This debonding phenomenon was also reported in the Broadgate building fire which had concrete slabs with steel decking [1]. The temperatures measured at 60 mm from the bottom of the trough lagged the SAFIR predictions for most of the fire. The temperatures at 110 mm from the exposed face generally showed good agreement with the measured temperatures. SAFIR was unable to model the temperature plateau at 100 °C at 60 and 110 mm, which was due to moisture effects.

5.3.2. Structural analysis

Fig. 20 shows a schematic of the structural representation of the *Hi-bond* slab. The flat deck of the slab was modelled with shell elements with different levels of fire exposure to represent the temperatures in the thin and thick sections, as described above. The trough of the slab, which consists of concrete and the steel decking, was modelled with a beam element in two parts, with concrete and steel properties in the lower half and non-load-bearing properties in the upper half (so that it does not contribute to the strength and stiffness of the slab, which is already provided by the shell elements). The nodeline of the beam element was aligned with those of the shell elements to simulate composite action between the beam and shell elements. Fig. 21 shows the plan view of the finite-element mesh for the *Hi-bond* slab. The analysis was performed for a quarter of the slab.

Fig. 22 compares the midspan deflections from the fire test with the deflections predicted using SAFIR for zero and 1.4 MPa ($0.25\sqrt{f'_c}$) concrete tensile strength.

The slabs with the two different concrete tensile strengths have similar deflection trends during the initial stages of the fire. The rapid deflection rates gradually decrease until they reach a constant and linear rate after about 45 min. The effect of different values of concrete tensile strength appears only after about 2 h of fire exposure.

SAFIR overpredicts the deflections because the analysis does not include the insulating effect of the debonded steel decking and the subsequent reduction of thermal bowing. At the advanced stages of the fire, the deflections are less sensitive to the thermal distribution and the numerical results show better agreement with the test results.

The analysis of the *Hi-bond* slab has shown that the temperatures and behaviour of the slab are difficult to predict if the debonding of the steel decking and the insulating effects of the layer of air between the slab and the steel deck are not taken into consideration. It would be possible to simulate the additional thermal resistance with a fictitious layer of insulating material but this would require more experimental validation. As debonding may not occur in every situation, it is conservative to ignore its effect for design purposes.

Fig. 18. Schematic of the composite section comprising beam and shell elements.

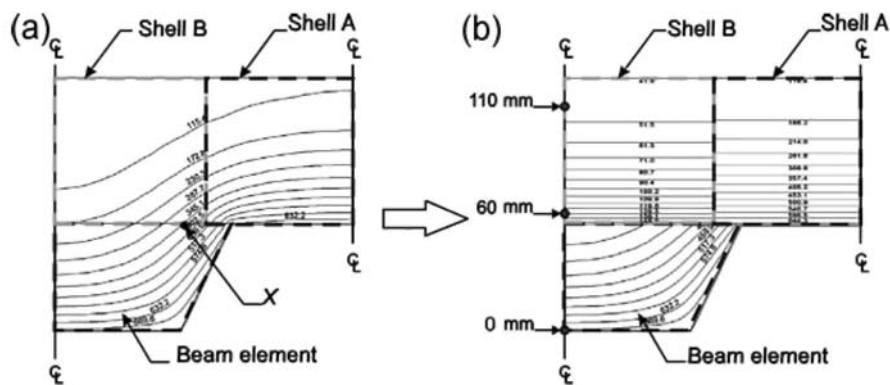


Fig. 19. Comparison of the measured and predicted temperatures in the Hi-bond slab.

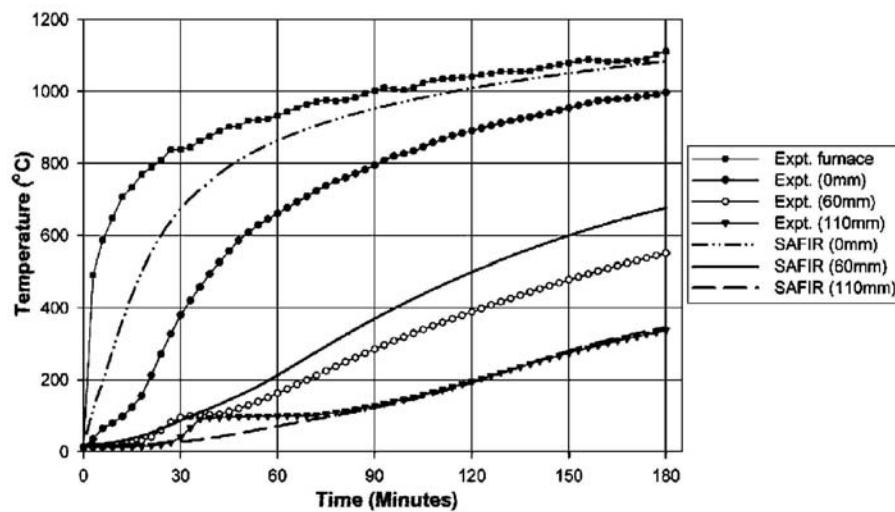


Fig. 20. Discretisation of the Hi-bond cross section for structural analysis.

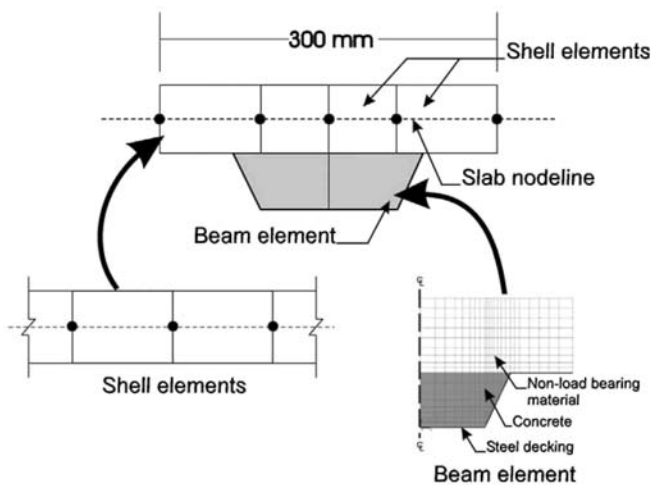


Fig. 21. Discretisation of the Hi-bond slab for structural analysis.

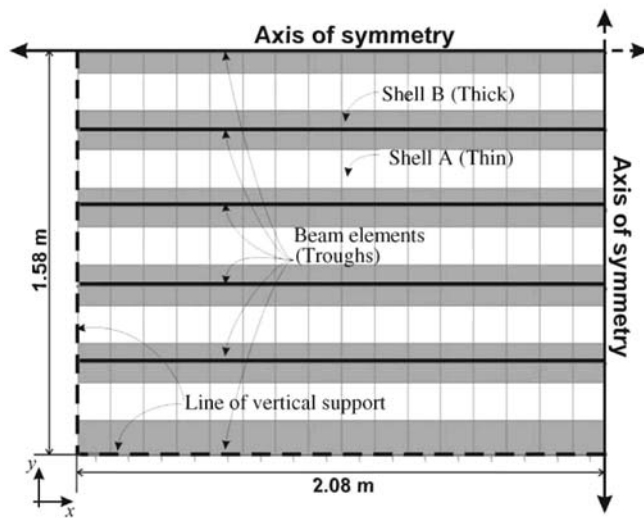
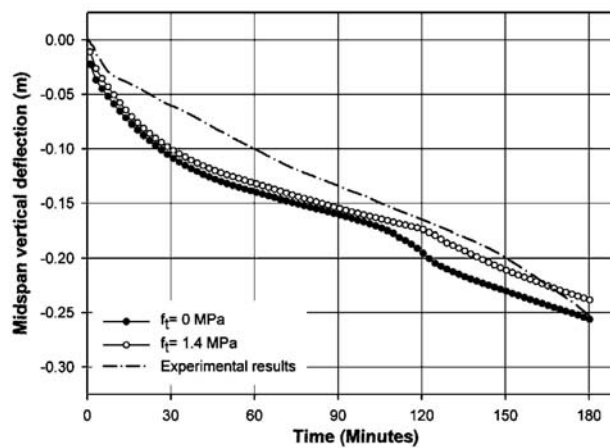


Fig. 22. Midspan vertical deflections of the Hi-bond slab during the ISO fire.



6. CONCLUSIONS

This paper describes the 3D analysis of two-way reinforced concrete slabs in fire conditions using a nonlinear finite-element program, SAFIR. The analysis was carried out using a new quadrilateral shell element with concrete properties. The properties of the shell element and the concrete model have been described briefly.

3D analysis of two-way reinforced concrete and composite slabs using the SAFIR shell element shows agreement with fire test results. Both the SAFIR analyses and the fire tests demonstrate that simply supported two-way slabs have excellent fire resistance provided that the slabs deform in double curvature and they have some support on all four edges. The analyses show that two-way slabs develop tensile membrane action in the initial stages of fire exposure, contributing to their good behaviour in fire.

The behaviour of composite slabs with steel decking is difficult to predict accurately unless the effects of debonding of the steel decking from the slab on the thermal distributions can be accounted for and modelled accurately.

Although beyond the scope of this study, the effects of restraint on two-way slabs should be studied as it would better represent the support conditions of real construction.

Acknowledgements

The authors acknowledge the support and funding provided by Colleen Wade of BRANZ, Geoff Bird of BHP New Zealand Steel Limited, Charles Clifton of the Heavy Engineering Research Association of New Zealand, and others.

References

- [1] Newman GM, Robinson JT, Bailey CG. Fire safe design: a new approach to multi-story steel-framed buildings. Berkshire (UK): The Steel Construction Institute; 2000.
- [2] Bailey CG, Lennon T, Moore DB. The behaviour of full-scale steel-framed buildings subjected to compartment fires. *The Structural Engineer* 1999;77(8):15-21.
- [3] Buchanan AH. Structural design for fire safety. UK: John Wiley & Sons Ltd; 2001.
- [4] Gillie M, Usmani A, Rotter M, O'Connor M. Modelling of heated composite floor slabs with reference to the Cardington experiments. *Fire Safety Journal* 2001;36(8):745-67.
- [5] Huang Z, Burgess IW, Plank RJ. Three-dimensional modelling of two full-scale fire tests on a composite building. *Proceedings of the Institution of Civil Engineers Structures and Buildings* 1999;134:243-55.
- [6] Huang Z, Burgess IW, Plank RJ. Non-linear modelling of three full-scale structural fire tests. *Proceedings of the First International Symposium of Structures in Fire, Copenhagen, 2000*, p. 53-70.
- [7] Huang Z, Burgess IW, Plank RJ. Non-linear structural modelling of a fire test subject to high restraint. *Fire Safety Journal* 2001;36(8):795-814.
- [8] Lamont S, Usmani AS, Drysdale DD. Fire protection of steel beams in composite framed structures. *Proceedings of the 2001 Interflam Conference, Edinburgh, 2001*, p. 407-18.
- [9] O'Callaghan DJ, O'Connor MA. Comparison of finite element models of composite steel framed buildings behaviour in fire. *Proceedings of the First International Symposium of Structures in Fire, Copenhagen, 2000*, p. 41-52.
- [10] Huang Z, Burgess IW, Plank RJ. Nonlinear analysis of reinforced concrete slabs subjected to fire. *ACI Structural Journal* 1999;96(1): 127-35.
- [11] Huang Z, Burgess IW, Plank RJ. Effective stiffness modelling of composite concrete slabs in fire. *Engineering Structures* 2000;22:1133-44.
- [12] Izzuddin BA, Elghazouli AY, Tao X. Realistic modelling of composite floor slabs under fire conditions. *Proceedings of 15th ASCE Engineering Mechanics Conference, June, New York, 2002*.

- [13] Gillie M, Usmani A, Rotter M, O'Connor M. Modelling of heated composite floor slabs with reference to the Cardington experiments. *Fire Safety Journal* 2001;36(8):745-67.
- [14] Lim L, Wade C. Experimental fire tests of two-way concrete slabs. *Fire Engineering Research Report 02/12*. University of Canterbury and BRANZ Ltd, New Zealand, 2002.
- [15] Lim L. Membrane action in fire exposed concrete floor systems. Ph.D. thesis, University of Canterbury, New Zealand, 2003.
- [16] Franssen JM. SAFIR: a thermal/structural program modelling structures under fire. *Proceedings of the North American Steel Construction Conference*, April, A.I.S.C. Inc., Baltimore, 2003.
- [17] Talamona D, Franssen JM. New quadrangular shell element in Safir. *Proceedings of the First International Symposium of Structures in Fire*, Copenhagen, 2000, p. 195-210.
- [18] Batoz JL, Tahar MB. Evaluation of a new quadrilateral thin plate bending element. *International Journal of Numerical Methods in Engineering* 1982;18:1655-77.
- [19] Ehm C, Schneider U. The high temperature behaviour of concrete under biaxial conditions. *Cement and Concrete Research* 1985;15(1):27-34.
- [20] Eurocode 2: Design of concrete structures. ENV 1992: Part 1-2: General rules—structural fire design. European Committee for Standardization, Brussels, 1995.
- [21] Talamona D, Franssen JM. A quadrangular shell finite element for concrete and steel structures subjected to fire. *Computers and Structures*, submitted for publication.
- [22] Vila Real PMM, Franssen JM. Lateral torsional buckling of steel I-beams in case of fire-numerical modelling. *Proceedings of the First International Symposium of Structures in Fire*, Copenhagen, 2000, p. 71-93.
- [23] Eurocode 3: Design of steel structures. ENV 1993 Part 1-2: General rules—structural fire design. European Committee for Standardization, Brussels, 1995.
- [24] Lamont S, Usmani AS, Drysdale DD. Heat transfer analysis of the composite slab in the Cardington frame fire tests. *Fire Safety Journal* 2001;36(8):815-39.